Digital Twin Design for hMSC Expansion in Hollow-fiber Bioreactors

Bharat Kanwar, Bryan Wang, Krishnendu Roy, Anirban Mazumdar, Senior Member, IEEE, and Stephen Balakirsky, Senior Member, IEEE

Abstract—Human Mesenchymal Stromal Cells (hMSC) have shown promising pre-clinical results by eliciting immunomodulatory effects to alleviate inflammation. In order to further study these effects, consistent and automated expansion platforms are required. Recent theoretical innovations have shown that model-based automated controls can more effectively regulate key nutrient concentrations. However, this previous work did not account for time-varying cell growth and death which resulted in inconsistent modeling and controller performance. To mitigate these effects, we propose a new model with timevarying parameters to track viable, proliferating, and dead cells and their respective growth rates with algorithms to estimate these parameters as functions of our limited measured states. We then propose an updated control architecture (referred to as smooth-controller) to leverage the additional parameters for improved estimation and control. The control objective is to regulate glucose and lactate to fixed setpoints while minimizing total media usage and large flowrate disturbances. Finally, we demonstrate the new control architecture in hMSC expansion with improved lactate setpoint MSE (58% reduction), improved observer MSE (36% for glucose and 20% for lactate), and reduced process disturbance (1 to 0 lactate spikes). Although the smooth-controller did not improve cell yield (4.91×10^7) compared to 5.08×10^7), it did reduce media usage to match the reduced growth rate thereby increasing cell yield per mL of fed media $(6.3 \times 10^4 \text{ to } 8.6 \times 10^4)$.

Index Terms—Cellular Dynamics, Estimation, Process Control

I. Introduction

Adult human Mesenchymal Stromal Cells (hMSCs) offer promising therapeutic effects for regenerative medicine. Pre-clinical studies have demonstrated immunomodulatory results from hMSC treatment for various indications [1]–[3]. Automated cell-expansion platforms and consistent quality cell products are necessary to scale up production to further study these clinical effects [4], [5].

Hollow-fiber bioreactors, such as the Quantum (Terumo BCT), are approved for cell manufacturing for clinical use to enable large-scale expansion of hMSCs [6]. Bioreactors

This work was sponsored by the U.S. Food and Drug Administration (FDA) under grant number R01FD006598.

Bharat Kanwar is with the Woodruff School of Mechanical Engineering at Georgia Tech, Atlanta, GA 30318 (email: bkanwar3@gatech.edu).

Bryan Wang is with the Wallace H Coulter Department of Biomedical Engineering at Georgia Tech, Atlanta, GA 30318 (email: bryanwang@gatech.edu).

Krishnendu Roy is with the Wallace H Coulter Department of Biomedical Engineering at Georgia Tech, Atlanta, GA 30318 (email: krishnendu.roy@bme.gatech.edu).

Anirban Mazumdar is with the Woodruff School of Mechanical Engineering at Georgia Tech, Atlanta, GA 30318 (email: anirban.mazumdar@me.gatech.edu).

Stephen Balakirsky is with the Georgia Tech Research Institute, Atlanta, GA 30318 (email: stephen.balakirsky@gtri.gatech.edu).

attempt to regulate the many relevant processes and environmental parameters in the cell expansion process. Currently, these quantities are regulated with intermittent intervention from skilled operators to measure nutrient values and update flowrates [7]. This method results in slow feedback rates, limited knowledge of full system dynamics, and increased variability. Automated control and modeling techniques have been proposed for MSC growth [8], [9] but have so far been limited to small-scale, static culture vessels without model-based control techniques to account for varying culture conditions.

In our prior work, we proposed a novel automated control system and control-centric model to address these limitations [10]. The key contributions of this work are 1) updating the control-centric model with updated fluid dynamics parameters and time-varying cell dynamics, 2) designing an estimation model for cell count and cell growth rate parameters, 3) formulating a multiple observer model that accounts for new sensing frequency limitations and estimates both unmeasurable states and model parameters, 4) upgrading the state feedback controller to improve glucose and lactate regulation while minimizing observer errors, and 5) show that the updated estimation and control architecture improves cell yield per mL fed media over the prior control architecture in cell expansion (Fig. 1).

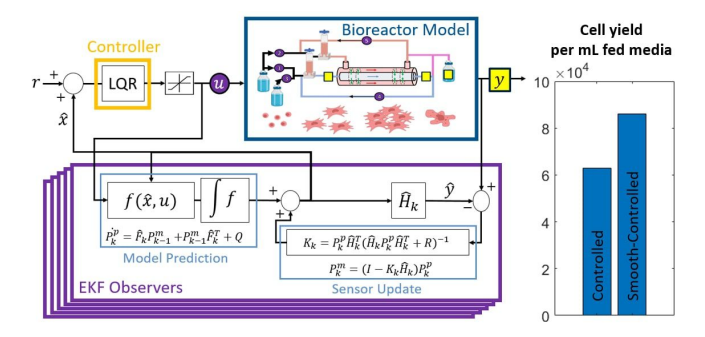


Fig. 1: Control architecture with updated fluid model, cell model, observer, and controller enables improved cell yield per mL fed media in expansion.

II. BIOREACTOR SYSTEM OVERVIEW

As in the prior bioreactor overview in [10], the primary control goal is to regulate the concentrations of glucose and lactate within the bioreactor while minimizing process disturbances and media usage. The bioreactor setup also remains largely the same, with our medium-scale hollow-fiber bioreactor's intra-capillary (IC) space as a bundle of

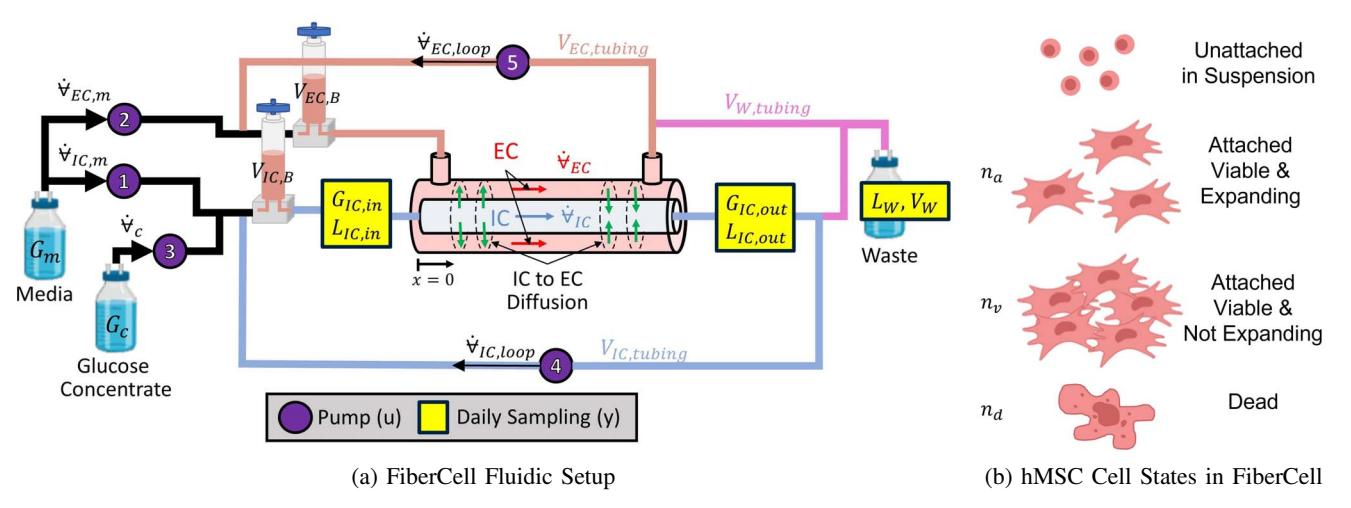


Fig. 2: Overview of bioreactor model with updated fluid dynamics (a) and cell dynamics (b).

semi-permeable fiber membrane tubes in which hMSCs are seeded, and an extra-capillary space (EC) which allows for parallel media flow and nutrient exchange. The same media and glucose concentrate solutions are used to perfuse across the cells and replenish nutrients/remove waste during the expansion process. Peristaltic pumps are used for all five actuators shown in Fig. 2a.

Our updated bioreactor system introduced new fluid dynamics in the form of modified IC and EC flow loops with reduced volumes. This reduced the required loop flowrates. It also introduced 5 mL dead volumes in the IC and EC loops which trap bubbles out of the bioreactor, and reduce input nutrient concentration spikes. In-line continuous glucose and lactate sensors were replaced with daily at-line sampling of glucose and lactate at the inlet and outlet due to inconsistency of sensor calibration and long-term inaccuracy of data. Additional daily measurements of waste media lactate and volume were also taken for improved observer performance. This updated bioreactor setup is shown in Fig. 3 and is used for experimental cell expansion results.

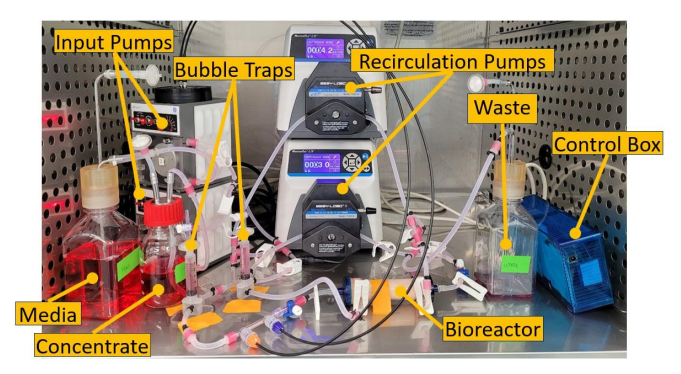


Fig. 3: Bioreactor Setup used for cell expansions.

In this work we compare the performance of our new automated control architecture (smooth-controlled) with both a baseline manual expansion protocol (baseline) and our prior automated control architecture (controlled).

All three protocols start with coating and seeding the

bioreactor. After this step, the baseline protocol introduces a minimal level of perfusion for the first 2 days of expansion, first through EC, then through IC, and doubles flowrates every day after that until the end of the expansion on day 6. The controlled protocol follows the same baseline protocol until day 3 after which the controller regulates input media and concentrate flowrates. In contrast, the smooth-controller begins perfusion on day 1 itself with setpoints fixed at the day 1 glucose and lactate measurement levels. All protocols are also limited to 1L of media for perfusion. The protocols are compared with the following metrics: Glucose and lactate setpoint mean squared error (S-MSE), Glucose and Lactate observer mean-squared error (O-MSE), media usage, number of lactate spikes, and final cell yield.

III. DIGITAL TWIN MODEL

In order to implement automated feedback process control we first design a digital model for the physical plant (our medium-scale hollow-fiber bioreactor) that accurately simulates the system inputs (media flowrates), in-process measurements (glucose and lactate), and cell counts in real-time. We also apply optimal estimation and control algorithms in real-time to interface with the physical plant and control for specific process parameters. This procedure has been documented for other bio-manufacturing processes under a digital-twin modeling framework [11]. This modeling task is split up into a fluid dynamics model, a cell dynamics model, a cell expansion estimation model, an observer model for optimal estimation, and a controller.

A. Fluid Dynamics Model

The fluid dynamics model of the bioreactor describes how concentrations of glucose and lactate vary due to bioreactor design/geometry and media flowrates. The IC and EC states for the hollow-fiber bioreactor were designed and validated in our prior work and the dynamics describing the convection diffusion model for glucose and lactate are shown below:

$$\frac{\partial G}{\partial t} = D_G \frac{\partial^2 G}{\partial x^2} + \frac{\dot{\forall}}{A} \frac{\partial G}{\partial x} + K_{ICEC} \frac{\partial^2 G_{ICEC}}{\partial r^2} + G_c n_a \tag{1}$$

$$\frac{\partial L}{\partial t} = D_L \frac{\partial^2 L}{\partial x^2} + \frac{\dot{\forall}}{A} \frac{\partial L}{\partial x} + K_{ICEC} \frac{\partial^2 L_{ICEC}}{\partial r^2} + L_p n_a \quad (2)$$

The parameter determination, discretization, and model validation are described in more detail in [10].

The updated bioreactor setup in Fig. 2a introduces new tubing volumes, $V_{IC,tubing} = 0.01$ L, $V_{EC,tubing} = 0.025$ L, and $V_{W,tubing} = 0.01$ L. For the flowrates studied in this experiment, the volumes were sufficiently mixed with minimal gradients when simulated. Therefore, these volumes were modeled as continuously mixed, so like with the sensor and tubing states in [10], a mixed-tank linear model was used for these additional volumes.

The new dead volumes, $V_{IC,B}$ and $V_{EC,B}$, were not necessarily constant during the expansion as media evaporates and bubbles get trapped in the dead volume. In application however, the dead volume states were modeled as constant (at 0.004L) due to the back-pressure from the hollowfiber bioreactor filling up the volumes, and could therefore also use the mixed-tank linear model approach.

The evaporated media and bubble volume then resulted in reduced waste bottle volume. Ordinarily this evaporation rate would need to be modeled. However, the waste bottle measurement serves the specific model purpose of determining the cumulative lactate quantity (mg) in the waste bottle, which would not be affected by evaporation and bubbles. Therefore, the newly added waste bottle states, V_W and L_W , were also modeled using the mixed-tank linear model as follows:

$$\frac{dV_W}{dt} = \dot{\forall}_{IC,m} + \dot{\forall}_{EC,m} + \dot{\forall}_c \tag{3}$$

$$\frac{dL_W}{dt} = \frac{L_{W,tubing}}{V_W} (\dot{\forall}_{IC,m} + \dot{\forall}_{EC,m} + \dot{\forall}_c) \tag{4}$$

B. Cell Dynamics Model

In [10], glucose consumption and lactate production terms were driven by a simple exponential growth function for cell number with constant cell growth rate, glucose consumption rate and lactate production rate. More advanced metabolic flux models (DFBA) have been proposed for fermentation processes where there is enough metabolic and gene data to correlate with growth rate [12]. Some such models have been developed for MSCs in static cultures [13], [14] but not for our bioreactor environment. With future metabolic analysis of bioreactor expansions, a similar flux model could be determined for our system. In this paper, we only considered glucose and lactate fluxes as our controllable metabolites and improved this simpler flux model to account for varying growth parameters and growth phases.

The main parameters/states of interest for this improved cell model (Fig 2b) are as follows:

$$\theta = [n_v; n_a; n_d; C_\sigma; C_d] \tag{5}$$

with total viable cells (n_v) , attached/actively growing cells (n_a) , dead cells (n_d) , cell growth rate (C_g) and cell death rate (C_d) .

For cell growth dynamics, we split this model into two distinct phases, growth during attachment and growth after attachment.

The attachment phase occurs right after cells are seeded into the bioreactor, at which point all elements of θ are 0. Static hMSC culture indicates that the attachment occurs at a negative exponential rate [15], where 60-90% of the attachment occurs in the first 5 hours and 100% attachment occurs at 24 hrs. This is captured by the following differential equation:

$$\frac{dn_a}{dt} = \frac{n_{seeded}}{14400} e^{-t/14400} \tag{6}$$

where n_{seeded} is the number of suspended cells introduced into the bioreactor.

Once the cells attach, they begin proliferating, consuming glucose and producing lactate. This is modeled proportional to the attachment negative exponential with the final cell growth rate being the initialized growth rate value from a prior baseline expansion (C^0_σ) :

$$\frac{dC_g}{dt} = \frac{C_g^0}{14400}e^{-t/14400} \tag{7}$$

The attachment phase ends when $n_a \ge 0.99n_{seeded}$.

After the attachment phase, cell growth rate starts to drive the majority of the glucose decrease and lactate increase in the bioreactor. To compute n_a in this phase, we must first account for cell confluency (C_c) , computed as the fraction of attached MSC surface area (S_C) to available fiber surface area (S_f) , which can inhibit expansion at high cell densities. This assumes even distribution of cells across the fibers.

$$C_c = \frac{n_v S_C}{S_f} \tag{8}$$

Cells are mobile during growth and will aim to expand into empty space, so with an even initial seeding, the confluency should be relatively uniform across fibers. MSCs are typically harvested at 70-80% confluency [16]. With this notion, we compute n_a or the number of attached cells that can double given the available surface area as follows:

$$n_{a} = \begin{cases} n_{v} & \text{if } 0 \le C_{c} < 0.5\\ (0.8 - C_{c})n_{v} & \text{if } 0.5 \le C_{c} < 0.8\\ & \text{else harvest cells} \end{cases}$$
(9)

Figure 2b highlights this confluency effect which differentiates n_a from n_v .

In this growth phase after attachment, the following differential equation tracks the total number of viable cells (n_v) ,

$$\frac{dn_v}{dt} = n_a(C_g - C_d) \tag{10}$$

High confluency, pressure, and shear stress can influence cell death [17], however our current experimental protocol aims for 80% confluency at harvest to prevent cell death due to overcrowding while minimizing input flowrates to reduce the effects of changing pressure and shear stress. Therefore cell death is assumed to be negligible for the following simulations and expansions.

C. Fluid and Cell Model Validation

The new fluid dynamic and cell dynamic models were validated with a preliminary controlled cell expansion. The cell model parameters were initialized to the rates observed in prior baseline expansions. Measurements of the input and output glucose and lactate concentrations were taken and compared to the fitted model (Fig. 4):

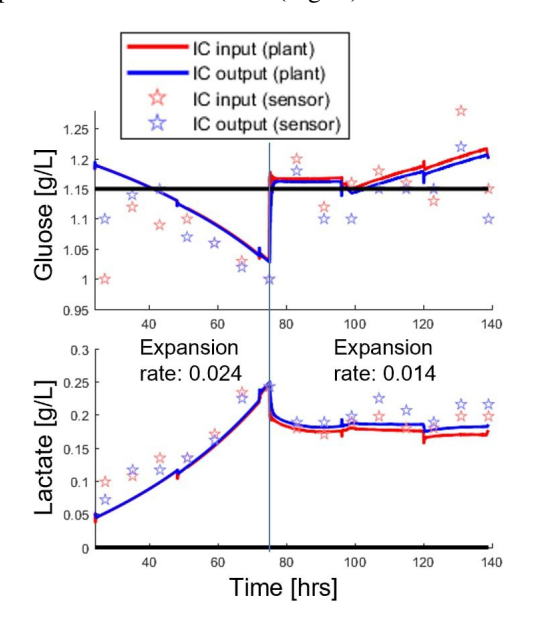


Fig. 4: Model validation with post-expansion fitted C_{ϱ} model

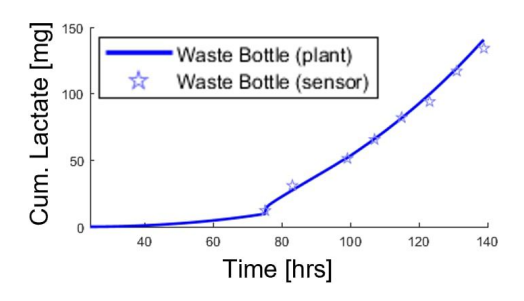


Fig. 5: Model validation of waste cumulative lactate with with post-expansion fitted C_g model

Additionally, with this best-fit parameter model, the waste cumulative lactate (defined as $V_w L_w$) was simulated and compared with the measured lactate concentrations and volumes in the waste bottle (Fig. 5) with a best-fit MSE of 0.011mg for waste cumulative lactate.

From Fig. 4 it is clear that the best-fit model for C_g required transient cell growth rate, which necessitates either a future dynamic model for C_g (such as DFBA for MSCs) or an effective estimator, which we propose in the following section. With the exception of the C_g parameter all other fluid and cell model parameters were validated.

D. Cell Expansion Estimation Model

As we illustrated in the previous section, incorrect cell model assumptions, especially with infrequent samples, can result in reduced predictive accuracy. Therefore, the cell dynamics model was further extended to explore cell growth rate and cell number estimation based on in-process metabolite measurements. Similar work has been conducted with perfusion-based bioreactors to correlate lactate mass-flux to measured cell number [9]. However, this fitted correlation model is limited because it relies on accurate and frequent lactate measurements without allowing for cell growth rate estimation for forward simulation. Our proposed dynamic model addresses both issues.

Since our bioreactor is a closed system, all lactate present in the reactor, tubing, and waste must have been produced by cells in the bioreactor. With the addition of the waste bottle sensed states we can estimate the cumulative lactate at sample-time k:

$$\begin{split} L_{cum}^{k} = & L_{w}V_{w} + L_{IC,out}V_{W,tubing} + L_{IC,out}V_{W,tubing} \\ & + \frac{L_{IC,in} + L_{IC,out}}{2} \\ & (V_{IC,tubing} + V_{EC,tubing} + V_{IC,B} + V_{EC,B}) \end{split} \tag{11}$$

This computation cannot take advantage of the estimated states since those are based on potentially incorrect model assumptions.

In order to compute cell growth rate, an equation is needed to relate cumulative lactate, cell growth rate, and viable cell number shown below:

$$L_{cum}^{k} = \alpha \frac{L_{p} n_{v}^{k}}{C_{g}^{k-1}} \left(e^{C_{g}^{k-1} (t^{k} - t^{k-1})} - 1 \right) + L_{cum}^{k-1}$$
 (12)

$$n_v^k = n_v^{k-1} e^{C_g^{k-1}(t^k - t^{k-1})}$$
(13)

where C_g and n_v are initialized to the baseline fitted cell growth rate and the initial seeded cell number respectively. Equation 12 can be considered a pseudo-sensor for C_g^{k-1} and can be solved by using Newton-Raphson root-finding methods. Equation 13 is also a pseudo-sensor for n_v^k as a function of the solution of Equation 12 for C_g^{k-1} .

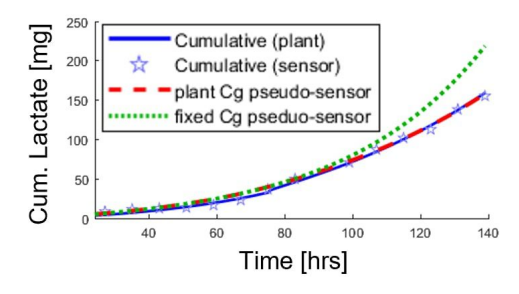


Fig. 6: Model validation of cumulative lactate dynamic model and $C_{\rm g}$ sensor model

The same bioreactor expansion shown in Fig. 4 was used to validate the cumulative lactate pseudo-sensor. Fig. 6 shows Equation 12 plotted with the "true" cell growth parameters as the plant Cg pseudo-sensor, while the observer Cg pseudo-sensor equation assumes that the cell growth rate stayed constant at the initialized value for the entire expansion.

The plant Cg pseudo-sensor also matched well with the computed cumulative data (MSE of 0.011mg), although there was some variance attributed to the lactate sensor and volume measurement noise.

E. Observer Model

The above fluid dynamics, cell dynamics and cell estimation models enumerate many states that cannot be directly measured. Concentrations and cell counts within the IC fibers or the EC space cannot be accessed due to sterility concerns. Meanwhile, input/output states can be accessed for measurement, but continuous flow-through sensors were inaccurate and inconsistent, while manual measurements were limited to daily sampling of 1-2 mL to prevent unnecessary cell disturbance. These manual samples are also affected by temperature which can result in noisy/inaccurate measurements. Therefore it is important to design a state/parameter estimation model that can leverage limited sensing of the bioreactor to best estimate the value of the remaining model states.

In the previous sections, model equations were defined for all of the glucose, lactate and cell states (X), cell model parameters (θ) (shown in equation (5)), and input flowrates (u). In [10], a noise-optimal state estimate problem was already posited for the glucose and lactate concentration states X. By adding the discretized parameters θ as additional states for the observer architecture to track, we use the same extended kalman filter (EKF) design to compute noise-optimal estimated parameters in real-time.

However, these added parameters θ nearly double the number of states which results in an unstable EKF model due to the ill-conditioned inverse caused by the variance matrix (P) described in [10]. In order to combat this issue, a multiple partial EKF model was designed which groups together only the relevant states for estimation for each observer. Four independent observers were designed to estimate the following sets of states: 1) glucose IC, EC, and tubing, 2) lactate IC, EC, tubing, and waste, 3) cell growth rate (C_g), and 4) number of viable cells (n_v)

The glucose and lactate IC and EC observers both use a diagonal R matrix with sensor noise of 0.1 g/L and a diagonal Q matrix with model noise of 0.001 g/L for best tracking response, very similar to prior work. The waste volume is currently measured visually with a precision of 25 mL, which is used as the diagonal entry in the lactate R matrix.

The cell growth rate observer's R value should be calculated from the measured lactate states, however this value in the pseudo-sensor (Equation 12) is very unstable for small changes in concentration, so for practicality a value of 0.01/hr was used. The corresponding model Q value was set to 0.005/hr and the initialized variance was set to 1.

The viable cell number observer R value used the propagated C_g R value through the n_v pseudo-sensor (Equation 13 and the Q value was set to 10^5

F. Feedback Controller

In this work we use a Linear Quadratic Regulator (LQR) controller in a manner similar to our previous work [10].

LQR is an optimal control scheme that weights desired state costs against input costs which perfectly matches the control objectives to minimize glucose and lactate state setpoint errors while minimizing media usage. This was used to automatically update input bioreactor flowrates at 1 Hz. We improve on our prior system by linearizing and reoptimizing the feedback gains once per day after the in-line sensor measurements are taken. This is necessary because our new model has continuously changing parameters. The linearization and gains computation were carried out on an Intel NUC 8 running Ubuntu 16.04 in 0.543 seconds which is well within the control frequency.

The same Q_{LQR} and R_{LQR} matrices were used as in [10] for glucose and lactate state costs and input costs respectively. These values are shown below for Q_{LQR} :

$$G_{IC,in}: q = 50$$
 $L_{IC,in}: q = 50$ $G_{IC,cell}(l): q = 10^5$ $L_{IC,cell}(l): q = 10^5$ $L_{out}: q = 5 \times 10^5$ $L_{out}: q = 5 \times 10^5$ $L_{EC,in}: q = 10^5$ (14)

and R_{LOR} :

$$R_{LQR} = \begin{bmatrix} 10 & 0 & 0 & 0 & 0 \\ 0 & 10 & 0 & 0 & 0 \\ 0 & 0 & 1 & 0 & 0 \\ 0 & 0 & 0 & 0.01 & 0 \\ 0 & 0 & 0 & 0 & 0.01 \end{bmatrix}$$
 (15)

However, with the addition of the discretized parameters θ , additional matrix terms were defined as follows in the LQR optimization problem for cost J:

$$J = \int_0^\infty \left[\begin{bmatrix} X^T \theta^T u^T \end{bmatrix} \begin{bmatrix} Q_{LQR} & 0 & 0 \\ 0 & Q_{\theta} & N_{LQR} \\ 0 & N_{LQR}^T & R_{LQR} \end{bmatrix} \begin{bmatrix} X \\ \theta \\ u \end{bmatrix} \right] dt$$
(16)

The Q_{θ} matrix is 0 except for the n_v terms which are equal to 3×10^{-7} . The N_{LQR} matrix is 0 except for the $n_v \times \dot{\forall}_{IC,m}, \dot{\forall}_{EC,m}$ terms which are equal to $-n_{seeded}$. These two terms combine together to drive the cost down to 0 only if the control effort u increases exponentially to match the exponentially increasing n_v during the expansion. This addition removes the need for a feedforward controller. The complete updated control architecture is shown in Fig. 1.

IV. RESULTS

A. Simulation Results

Each system started with the same initial cell number, glucose and lactate concentrations, and flowrates. Simulations ended once the 80% confluence limit was reached (~ 6 days). The updated bioreactor physical parameters, cell behavior parameters, and the initial conditions are summarized in Table I and match the initialized parameters of the model validation expansion shown in Fig. 4.

The simulation of the digital twin model and feedback controller was developed in MATLAB. The EKF observer and LOR controller were also simulated using the sensed

$S_c[\mu m^2]$ [18]	~ 1000
$S_f[m^2]$	0.30
$C_g^0[1/hr]$	~ 0.021
$G_c[mg/(cell * hr)]$	$\sim -2 \times 10^{-8}$
$L_p[mmol/(cell*hr)]$	$\sim 2.8 \times 10^{-10}$
n _{seeded}	3×10^6 cells
Media glucose, lactate	1.15 g/L , 0.0 g/L
Concentrate glucose, lactate	~ 1.8 g/L, 0.0 g/L
$\dot{\forall}_{IC,loop}, \dot{\forall}_{EC,loop}$	3.2 mL/min , 4.0 mL/min

TABLE I: Simulation Parameters

states, sensing sampling rates (once per day), sensor noise, and controller update rates (1 Hz). The simulation results are shown in Table II.

	Baseline	Controlled	Smooth- Controlled
S-MSE Glucose [g/L]	0.026	0.010	0.009
S-MSE Lactate [g/L]	0.038	0.032	0.029
O-MSE Gluc./Lac. [g/L]	3×10^{-5}	1×10^{-5}	1.5×10^{-5}
Media [L]	0.920	0.812	0.823
Concentrate [L]	0.000	0.152	0.135
# Lactate Spikes	3	1	0

TABLE II: Simulation Results

B. Expansion Results

In addition to the model validation controlled bioreactor expansion (Expansion 1), a second bioreactor expansion (Expansion 2) was performed using the same initialized parameters shown in Table I and the same cell/reagent lots in the model validation expansion (Fig. 4). This second expansion implemented our updated real-time control architecture, novel parameter estimation model, smooth controller, and updated glucose and lactate setpoints (1.12 g/L and 0.1 g/L respectively) to eliminate error discontinuities. The second bioreactor expansion results are shown in Fig. 7 for glucose (7a), lactate (7b), cell number (7c), and cell growth rate (7d). Controller and observer performance metrics as well as media usage and total cell yield are shown in Table III comparing the two bioreactor expansions. The observer cell yield in Fig. 7c (4.6×10^7) is also within 6% of the true cell yield (4.91×10^7) .

	Expansion 1 (controlled)		Expansion 2 (smooth-controlled)	
	Glucose	Lactate	Glucose	Lactate
S-MSE [g/L]	0.01	0.03	0.01	0.01
O-MSE [g/L]	3.9×10^{-3}	1.2×10^{-3}	2.5×10^{-3}	9.6×10^{-4}
Media [L]	0.660		0.380	
Conc. [L]	0.150		0.190	
# Spikes	1		0	
Cell Yield	5.08×10^{7}		4.91×10^{7}	

TABLE III: Bioreactor Expansion Results

V. DISCUSSION

The simulation results show that the controlled case improved glucose and lactate setpoint MSE compared to the

baseline while the smooth-controlled case improved setpoint MSE compared to both controlled and baseline. Moreover, the large flowrate spike in the controlled case, reflected in the sudden nutrient spike in the model validation expansion (Fig. 4), was eliminated in the smooth-controlled case. We hypothesize this will maintain a more steady cell growth rate.

Comparing the bioreactor expansion results, expansion 2 improved lactate setpoint MSE (58% reduction), while also significantly reducing observer MSE (36% for glucose and 20% for lactate). The improved observer MSE especially implies that the cell growth rate and cell number estimation were accurate. Although expansion 2 did not maintain a higher cell growth rate or result in a higher cell yield than expansion 1, the accurate parameter estimation resulted in less control effort and a large increase in cell yield per mL fed media (6.3×10⁴ cells/mL compared to 8.6×10⁴ cells/mL).

Although our specific choice of reference profiles and control parameters did not increase cell number or growth rate, our designed control architecture enables novel future studies to optimize for these parameters. One such study is the impact of specific flowrates and flowrate trajectories on cell growth rate to enable direct regulation. Another study could evaluate the impact of different glucose and lactate reference profiles on cell growth rate.

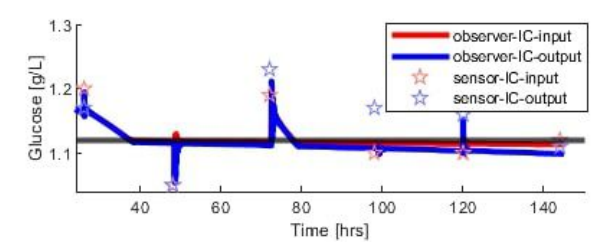
These future studies could also contribute to data-driven model expansion. Model predictive control (MPC) specifically has been used for cell growth prediction in small-scale static cultures [8] and would improve on our current estimation model which cannot predict parameter trajectories. We can leverage post-expansion cell quality assays for MSC function such as IDO suppression [19], macrophage M1 suppression [20], and T-cell co-culture [21] to determine key metabolites and cytokines to add to the model. With this detailed metabolite and quality data incorporated into an MPC algorithm, it might be possible to predict and regulate MSC cell growth parameters and quality assay metrics directly through correlative models like DFBA.

ACKNOWLEDGMENT

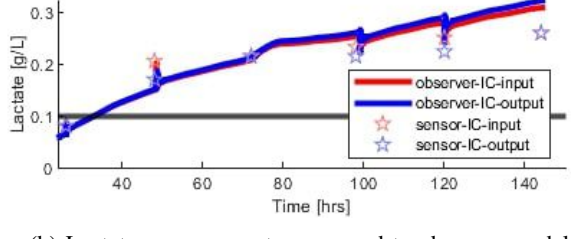
The authors of this paper would like to thank Annie Bowles and Carolyn Yeago for their cell-biology expertise.

REFERENCES

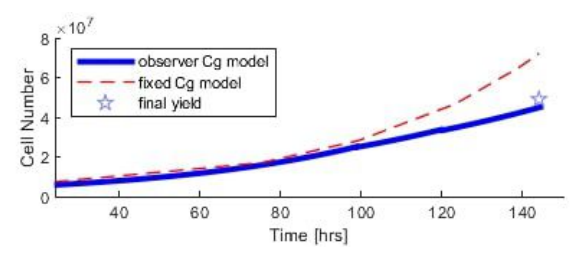
- K. Le Blanc, I. Rasmusson, B. Sundberg, C. Götherström, M. Hassan, M. Uzunel, and O. Ringdén, "Treatment of severe acute graft-versushost disease with third party haploidentical mesenchymal stem cells," Lancet, vol. 363, pp. 1439–1441, May 2004.
- [2] I. Molendijk, B. A. Bonsing, H. Roelofs, K. C. M. J. Peeters, M. N. J. M. Wasser, G. Dijkstra, C. J. van der Woude, M. Duijvestein, R. A. Veenendaal, J.-J. Zwaginga, H. W. Verspaget, W. E. Fibbe, A. E. van der Meulen-de Jong, and D. W. Hommes, "Allogeneic bone marrow-derived mesenchymal stromal cells promote healing of refractory perianal fistulas in patients with crohn's disease," <u>Gastroenterology</u>, vol. 149, pp. 918–27.e6, Oct. 2015.
- [3] J. Panés, D. García-Olmo, G. Van Assche, J. F. Colombel, W. Reinisch, D. C. Baumgart, A. Dignass, M. Nachury, M. Ferrante, L. Kazemi-Shirazi, J. C. Grimaud, F. de la Portilla, E. Goldin, M. P. Richard, A. Leselbaum, S. Danese, and ADMIRE CD Study Group Collaborators, "Expanded allogeneic adipose-derived mesenchymal stem cells (cx601) for complex perianal fistulas in crohn's disease: a phase 3 randomised, double-blind controlled trial," <u>Lancet</u>, vol. 388, pp. 1281–1290, Sept. 2016.



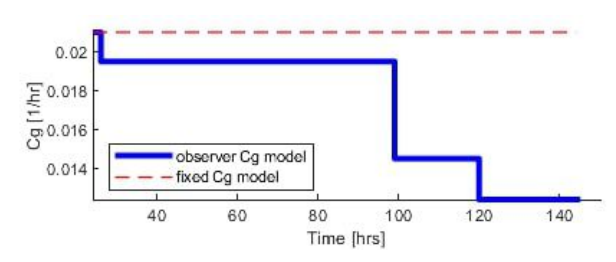
(a) Glucose measurements compared to observer model



(b) Lactate measurements compared to observer model



(c) Estimated cell number compared to final yield



(d) Estimated cell growth rate

Fig. 7: Bioreactor expansion with hMSCs using updated observer model for fluidic and estimated cell parameter states, and updated LQR controller.

- [4] A. Mizukami and K. Swiech, "Mesenchymal stromal cells: From discovery to manufacturing and commercialization," <u>Stem Cells Int.</u>, vol. 2018, p. 4083921, Apr. 2018.
- [5] M. Kabat, I. Bobkov, S. Kumar, and M. Grumet, "Trends in mesenchymal stem cell clinical trials 2004-2018: Is efficacy optimal in a narrow dose range?," <u>Stem Cells Transl. Med.</u>, vol. 9, pp. 17–27, Jan. 2020
- [6] C. Barckhausen, B. Rice, S. Baila, L. Sensebé, H. Schrezenmeier, P. Nold, H. Hackstein, and M. T. Rojewski, "GMP-Compliant Expansion of Clinical-Grade Human Mesenchymal Stromal/Stem Cells Using a Closed Hollow Fiber Bioreactor," <u>Methods in Molecular</u> <u>Biology</u> (Clifton, N.J.), vol. 1416, pp. 389–412, 2016.
- [7] A. L. Russell, R. C. Lefavor, and A. C. Zubair, "Characterization and cost-benefit analysis of automated bioreactor-expanded mesenchymal stem cells for clinical applications," <u>Transfusion</u>, vol. 58, pp. 2374– 2382, Oct. 2018.
- [8] K. Van Beylen, A. Youssef, A. Peña Fernández, T. Lambrechts, I. Papantoniou, and J.-M. Aerts, "Lactate-based model predictive control strategy of cell growth for cell therapy applications," <u>Bioengineering</u> (Basel), vol. 7, p. 78, July 2020.
- [9] R. B. Rice, R. Peters, B. Vang, M. Brecheisen, T. Startz, B. Nankervis, D. Windmiller, D. Antwiler, N. Givens, and M. E. Janssens, "Glucose and lactate measurements as a predictor of the human mesenchymal stem cell number in the quantum cell expansion system," 2012.
- [10] B. Kanwar, S. Balakirsky, and A. Mazumdar, "Modeling and Controller Design for Enhanced Hollow-fiber Bioreactor Performance," IEEE Control Systems Letters, pp. 1–1, 2021.
- [11] I. A. Udugama, P. C. Lopez, C. L. Gargalo, X. Li, C. Bayer, and K. V. Gernaey, "Digital twin in biomanufacturing: challenges and opportunities towards its implementation," <u>Systems Microbiology and</u> Biomanufacturing, 2021.
- [12] M. A. Henson and T. J. Hanly, "Dynamic flux balance analysis for synthetic microbial communities," <u>IET Syst. Biol.</u>, vol. 8, pp. 214– 229, Oct. 2014.
- [13] H. Fouladiha, S.-A. Marashi, M. A. Shokrgozar, M. Farokhi, and A. Atashi, "Applications of a metabolic network model of mesenchymal stem cells for controlling cell proliferation and differentiation," Cytotechnology, vol. 70, pp. 331–338, Feb. 2018.
- [14] H. Fouladiha, S.-A. Marashi, and M. A. Shokrgozar, "Reconstruction and validation of a constraint-based metabolic network model for bone marrow-derived mesenchymal stem cells," <u>Cell Prolif.</u>, vol. 48, pp. 475–485, Aug. 2015.

- [15] D. Salzig, J. Leber, K. Merkewitz, M. C. Lange, N. Köster, and P. Czer-mak, "Attachment, Growth, and Detachment of Human Mesenchymal Stem Cells in a Chemically Defined Medium," Feb. 2016.
- [16] F. A. M. Abo-Aziza and Z. A A, "The impact of confluence on bone marrow mesenchymal stem (BMMSC) proliferation and osteogenic differentiation," <u>Int. J. Hematol. Oncol. Stem Cell Res.</u>, vol. 11, pp. 121–132, Apr. 2017.
- [17] X. Yuan, T. M. Logan, and T. Ma, "Metabolism in Human Mesenchymal Stromal Cells: A Missing Link Between hMSC Biomanufacturing and Therapy?," Frontiers in Immunology, vol. 10, May 2019.
- [18] J. R. Smith, K. Pfeifer, F. Petry, N. Powell, J. Delzeit, and M. L. Weiss, "Standardizing umbilical cord mesenchymal stromal cells for translation to clinical use: Selection of GMP-compliant medium and a simplified isolation method," <u>Stem Cells Int.</u>, vol. 2016, p. 6810980, Feb. 2016.
- [19] O. DelaRosa, E. Lombardo, A. Beraza, P. Mancheño-Corvo, C. Ramirez, R. Menta, L. Rico, E. Camarillo, L. García, J. L. Abad, C. Trigueros, M. Delgado, and D. Büscher, "Requirement of IFN-gamma-mediated indoleamine 2,3-dioxygenase expression in the modulation of lymphocyte proliferation by human adipose-derived stem cells," <u>Tissue Eng. Part A</u>, vol. 15, pp. 2795–2806, Oct. 2009.
- [20] A. B. Vasandan, S. Jahnavi, C. Shashank, P. Prasad, A. Kumar, and S. J. Prasanna, "Human mesenchymal stem cells program macrophage plasticity by altering their metabolic status via a PGE2-dependent mechanism," <u>Sci. Rep.</u>, vol. 6, p. 38308, Dec. 2016.
- [21] D. D. Bloom, J. M. Centanni, N. Bhatia, C. A. Emler, D. Drier, G. E. Leverson, D. H. McKenna, Jr, A. P. Gee, R. Lindblad, D. J. Hei, and P. Hematti, "A reproducible immunopotency assay to measure mesenchymal stromal cell-mediated t-cell suppression," Cytotherapy, vol. 17, pp. 140–151, Feb. 2015.